Runx2 is required for hypertrophic chondrocyte mediated degradation of cartilage matrix during endochondral ossification

Harunur Rashid, Haiyan Chen and Amjad Javed *

Department of Oral and Maxillofacial Surgery, *Institute of Oral Health Research, School of Dentistry, University of Alabama at Birmingham, Birmingham, AL, USA*

Correspondence to Amjad Javed: Department of Oral and Maxillofacial Surgery, School of Dentistry SDB 714, University of Alabama at Birmingham, 1720 2ND Avenue South, Birmingham, AL 35294-0007, USA. *javeda@uab.edu (A. Javed)*
https://doi.org/10.1016/j.mbplus.2021.100088

Abstract

The RUNX2 transcription factor is a key regulator for the development of cartilage and bone. Global or resting chondrocyte-specific deletion of the *Runx2* gene results in failure of chondrocyte hypertrophy, endochondral ossification, and perinatal lethality. The terminally mature hypertrophic chondrocyte regulates critical steps of endochondral ossification. Importantly, expression of the *Runx2* gene starts in the resting chondrocyte and increases progressively, reaching the maximum level in hypertrophic chondrocytes. However, the RUNX2 role after chondrocyte hypertrophy remains unknown. To answer this question, we deleted the *Runx2* gene specifically in hypertrophic chondrocytes using the Col10-Cre line. Mice lacking the *Runx2* gene in hypertrophic chondrocytes ($Runx2^{HC/HC}$) survive but exhibit limb dwarfism. Interestingly, the length of the hypertrophic chondrocyte zone is doubled in the growth plate of $Runx2^{HC/HC}$ mice. Expression of pro-apoptotic *Bax* decreased significantly while anti-apoptotic *Bcl2* remains unchanged leading to a four-fold increase in the *Bcl2*/*Bax* ratio in mutant mice. In line with this, a significant reduction in apoptosis of $Runx2^{HC/HC}$ hypertrophic chondrocyte is noted. A large amount of cartilage matrix is present in the long bones that extend toward the diaphyseal region of $Runx2^{HC/HC}$ mice. This is not due to enhanced synthesis of the cartilage matrix as the expression of both collagen type 2 and aggrecan were comparable among $Runx2^{HC/HC}$ and WT littermates. Our qPCR analysis demonstrates the increased amount of cartilage matrix is due to impaired expression of cartilage degrading enzymes such as metalloproteinase and aggrecanase as well as tissue inhibitor of metalloproteinases. Moreover, a significant decrease of TRAP positive chondroclasts was noted along the cartilage islands in $Runx2^{HC/HC}$ mice. Consistently, qPCR data showed an 81% reduction in the *Rankl*/*Opg* ratio in $Runx2^{HC/HC}$ littermates, which is inhibitory for chondroclast differentiation. Finally, we assess if increase cartilage matrix in $Runx2^{HC/HC}$ mice serves as a template for bone and mineral deposition using micro-CT and Von Kossa. The mutant mice exhibit a significant increase in trabecular bone mass compared to littermates. In summary, our findings have uncovered a novel role of Runx2 in apoptosis of hypertrophic chondrocytes and degradation of cartilage matrix during endochondral ossification.

Introduction

The majority of the bones in the mammalian skeleton are generated through the process of endochondral ossification. This sequential process of bone formation starts with the condensation of mesenchyme during early embryonic development [1]. The SRY box transcription factor (SOX9) is required for the commitment of undifferentiated cells in the condensed mesenchyme to

chondrocytes [2,3]. The immature chondrocytes residing within the central regions of the hyaline cartilage primordia undergo proliferation and secrete the initial matrix which contributes to the growth of the cartilage template [4]. The hyaline cartilage is degraded by enzymes released from the hypertrophic chondrocytes and is eventually replaced with mineralized bone produced by osteoblasts [5,6].

During endochondral ossification, chondrocytes sequentially pass through resting, proliferative, prehypertrophic, and hypertrophic stages before undergoing apoptosis [7,8]. Chondrocytes in each stage are defined by unique morphology, arrangement, gene expression, and location within the growth plate [9]. The small resting chondrocyte expresses SOX9, parathyroid hormone-related peptide (PTHRP), collagen type II (COL2), and aggrecan (ACAN) [3,9–11]. During cartilage growth, resting chondrocytes undergo mitotic duplication with one daughter cell moving underneath the other, thereby resulting in the characteristic columnar arrangement of proliferative chondrocytes. The Cyclin-dependent kinase 1 (CDK1) and Wnt/planar cell polarity **(**Wnt/PCP) pathway regulate the development of proliferative chondrocytes characterized by the expression of cyclin d1 (CCND1) and Proliferating cell nuclear antigen (PCNA) [12–14]. The post-mitotic columnar chondrocyte transition to the prehypertrophic chondrocyte is marked by the expression of Indian hedgehog (IHH), PTHRP receptor (PTHRPR), and Runt related transcription factor 2 (RUNX2) [15–17]. Hypertrophic chondrocytes are the final stage in chondrocyte differentiation with a conspicuous expression of collagen type X (Col10), matrix metalloproteinase (MMP), aggrecanases (ADAMTS), and vascular endothelial growth factor-a (VEGFA) [17–19]. The sequential transition from the resting, proliferative to the hypertrophic stage is also regulated by extracellular signaling from BMP/TGFβ, FGF, NOTCH, and WNT/β-Catenin pathways [5,20–23].

The hypertrophic chondrocyte is the terminally mature and largest cell in the growth plate. Hypertrophic chondrocytes control angiogenesis, degradation of cartilage matrix, cartilage calcification, and differentiation of perichondral cells [4,8]. The VEGFA produced by the hypertrophic chondrocytes in response to hypoxia is an essential mediator of growth plate angiogenesis [18,24]. The vascular invasion facilitates the recruitment of progenitors for cartilage degrading chondroclasts and bone synthesizing osteoblasts [25]. Hypertrophic chondrocytes secrete aggrecanase, collagenase, and gelatinase that directly promote the degradation of the cartilage matrix [26,27]. Chondrocytes also express tissue inhibitor of matrix metalloproteinase (TIMPs) that inhibits the activity of these enzymes [28–31]. In addition, hypertrophic chondrocytes control the differentiation of the cartilage resorbing chondroclasts by releasing receptor activator of nuclear factor Kappa B ligand (RANKL) and osteoprotegerin (OPG) [32]. Deletion of *Rankl* gene specifically from hypertrophic chondrocytes leads to retention of calcified cartilage [33]. Hypertrophic chondrocytes regulate cartilage calcification through membrane bound enzymes and secretion of matrix vesicles [34,35]. The chondrocyte secreted vesicles are enriched in tissue-nonspecific alkaline phosphatase (TNAP), inorganic phosphate, calcium ions, and several calcium binding proteins. Secreted or membrane bound TNAP hydrolyzes pyrophosphate into inorganic phosphate to induce calcification. Hypertrophic chondrocytes also induce differentiation of perichondral cells to osteoblasts and the development of bone collar through secretion of the IHH and BMP3 [15,36]. Thus, the hypertrophic chondrocyte plays a central role in initiating both cartilage degradation and bone formation during endochondral ossification.

The RUNX2 transcription factor is essential for skeletal development. Global deletion of the *Runx2* gene results in failure of both osteoblast and chondrocyte differentiation and lack of intramembranous and endochondral ossification [37–39]. Although *Runx2* expression starts in the early chondrocyte, its role in chondrocyte hypertrophic differentiation is most appreciated. To test the spatiotemporal role of *Runx2* during endochondral ossification, many laboratories employed transgenic approaches using mouse models to overexpress *Runx2* in resting and hypertrophic chondrocytes. Overexpression of *Runx2* in resting chondrocytes accelerates hypertrophic maturation, endochondral ossification, and ectopic mineralization of permanent cartilage [40,41]. In contrast, blocking endogenous *Runx2* function in resting chondrocytes by dominant negative Runx2 results in delayed chondrocyte hypertrophy and endochondral ossification [40]. Transient overexpression of *Runx2* in resting chondrocytes also causes accelerated hypertrophy, endochondral ossification, and apoptosis of chondrocytes [42]. Interestingly, overexpression of *Runx2* in hypertrophic chondrocytes delays chondrocyte hypertrophy, reduces mineralization and decreases chondrocyte apoptosis [43]. Overexpression of Runx2 in resting chondrocytes lead to perinatal lethality but mice overexpressing *Runx2* in hypertrophic chondrocytes survive [40,43]. Thus, overexpression models have failed to reveal the spatiotemporal role of the *Runx2* gene during endochondral ossification.

Both global and resting chondrocyte-specific *Runx2* null models show a complete lack of chondrocyte hypertrophy and endochondral ossification and lethality at birth [17,37,44]. The failed endochondral ossification in these models is attributed to the absence of chondrocyte hypertrophy. It is important to note that during chondrogenesis, expression of the *Runx2* gene starts in resting chondrocytes and increases progressively,

reaching the maximum level in hypertrophic chondrocytes. However, the physiologic role of the endogenous *Runx2* gene after chondrocyte hypertrophy remains unknown. We address this question by deleting the *Runx2* gene in hypertrophic chondrocytes using the BAC-Col10a-Cre transgenic model [45].

Results

Runx2 deletion in hypertrophic chondrocytes results in poorly mineralized extremities and limb dwarfism

To study the regulatory role of RUNX2 beyond chondrocyte hypertrophy, the *Runx2* gene was deleted in hypertrophic chondrocytes by mating a $Runx2^{F/F}$ mouse with BAC-Col10-Cre transgenic mouse. We confirmed that Col10-Cre activity is specific to the hypertrophic chondrocytes by using Ai9-tdTomato reporter mice (Fig. 1A). Histologic analysis of femurs from newborn mice showed tdTomato positive cells appearing in the last two rows of the hypertrophic zone and extending into the calcified cartilage (Fig. 1A). These data are consistent with the previously reported pattern of BAC-Col10-Cre gene expression only in hypertrophic chondrocytes [45].

Interestingly, homozygous mice ($Runx2^{HC/HC}$) are born alive with the expected Mendelian ratio and have comparable bodyweight to heterozygous ($Runx2^{+/HC}$) and wild-type ($Runx2^{+/+}$) littermates (Fig. 1B). Whole mount alizarin red and alcian blue staining revealed an overall well-formed skeleton, indicating the activity of the *Runx2* gene in the hypertrophic chondrocyte is not essential for embryonic skeletogenesis (data not shown). However, the total length of intact forelimb and hindlimb are significantly shorter in homozygous mice (Fig. 1C). We assessed contributions of the proximal, intermediate, and distal elements toward limb dwarfism by measuring the alizarin red stained regions among littermates (Fig. 1D, E). Quantification of the ossified region from seven

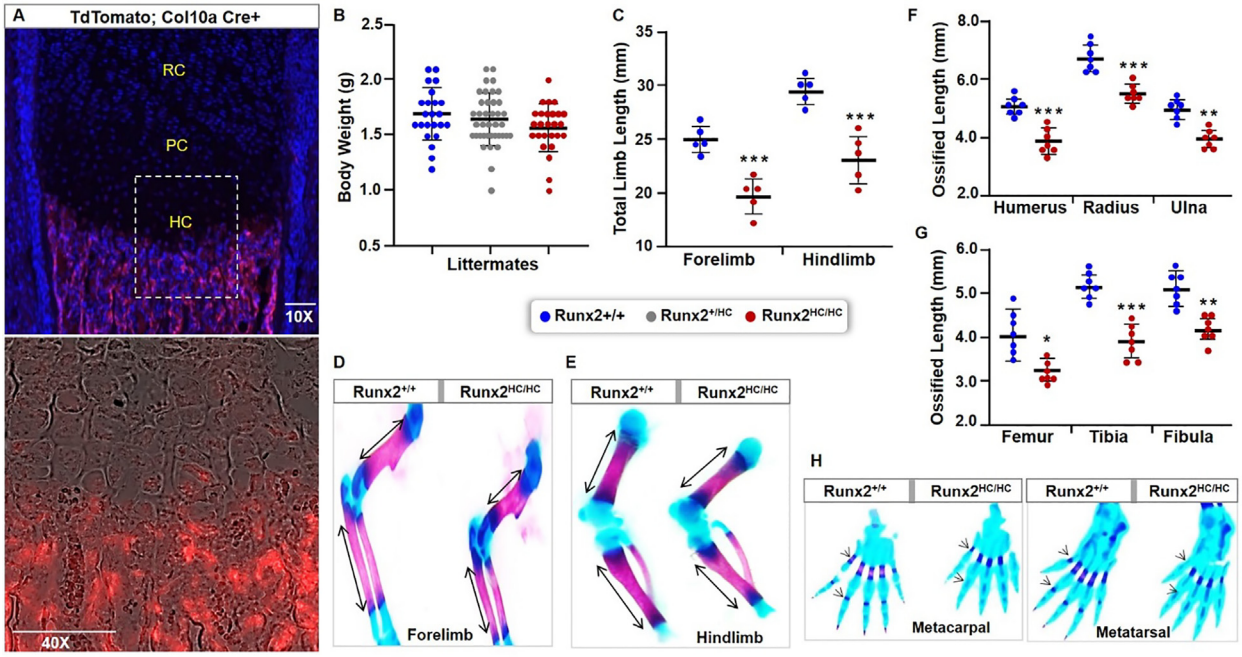

Fig. 1. Deletion of *Runx2* in hypertrophic chondrocytes results in decreased mineralization of limbs and extremities. (A) Cryo-section of the femur from a newborn pup containing BAC-Col10-Cre and ROSA26-tdTomato transgenes. A representative image with DAPI/TRITC overlay is shown at 10x magnification. The boxed region captured at 40X magnification is shown as phase contrast with TRITC overlay. RC: resting chondrocytes; PC: proliferative chondrocytes; HC: hypertrophic chondrocytes. Scale bar: 100 μm. (B) The whole-body weight of 3-days old littermates from multiple pregnancies are presented in a scatter plot. ($Runx2^{+/+}$ n = 23, $Runx2^{+/HC}$ n = 39, $Runx2^{HC/HC}$ n = 25). (C) The total length of intact forelimbs and hindlimbs from 3-days old $Runx2^{+/+}$ and $Runx2^{HC/HC}$ littermates is presented in the scatterplot plot (n = 5). (D, E) A representative image of alizarin red and alcian blue stained forelimbs and hindlimbs from $Runx2^{+/+}$ and $Runx2^{HC/HC}$ littermates. (F, G) The length of ossified regions in each element of the forelimb (humerus, radius, ulna) and the hindlimb (femur, tibia, and fibula) was measured digitally and presented in the scatter plot (n = 7). (H) A representative image of the hand and paw stained with alizarin red and alcian blue. Arrowheads indicate unmineralized digits in the metacarpal and metatarsal of the $Runx2^{HC/HC}$ mice. (*$P < 0.05$, **$P < 0.01$, ***$P < 0.001$). (For interpretation of the references to colour in this figure legend, the reader is referred to the web version of this article.)

littermates showed a 20% shorter length of the humerus and a 15% shortening of both radius and ulna in homozygous mice (Fig. 1F). Similarly, the length of the ossified regions in the femur, tibia, and fibula is reduced by 15% and 14% respectively. (Fig. 1G). Moreover, the distal elements (metacarpal and metatarsal) were unmineralized and the phalanges were poorly developed in *Runx2*$^{HC/HC}$ mice (Fig. 1H). Together these results demonstrate that *Runx2* loss in hypertrophic chondrocytes leads to limb dwarfism.

Runx2 deficiency in the hypertrophic chondrocyte leads to significant expansion of the zone of hypertrophy in the growth plate

To understand the effect of *Runx2* loss in hypertrophic chondrocytes during endochondral ossification, we performed histological analysis. H&E staining revealed that the overall length of the growth plate is increased significantly in the *Runx2*$^{HC/HC}$ mice (Fig. 2A). Quantification of growth plate length confirmed an increase of 14% at the proximal end and 12% at the distal end of the tibia (Fig. 2C). Surprisingly, the hypertrophic chondrocyte zone is enlarged in both the proximal and distal growth plate of the *Runx2*$^{HC/HC}$ littermates (Fig. 2A-B). Quantification of the length of hypertrophic chondrocyte zone showed an increase of 89% in proximal and 87% in the distal growth plate (Fig. 2D). The significant lengthening of the hypertrophic zone is also noted in the growth plate of the femur, metacarpal, and metatarsal of the *Runx2*$^{HC/HC}$ mice (data not shown). In contrast, the length of the bone region between the proximal and distal growth plate in the tibia is decreased by 32% in the *Runx2*$^{HC/HC}$ littermates (Fig. 2A, E).

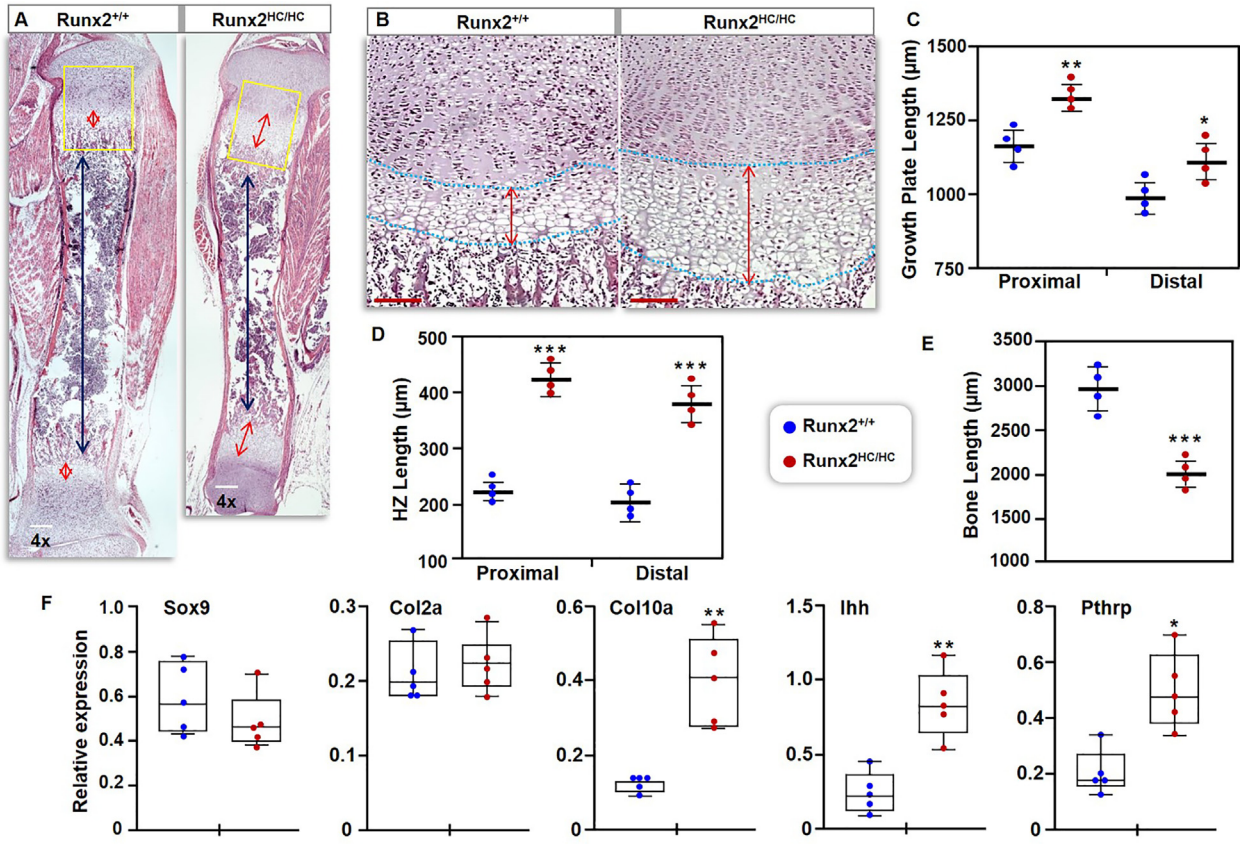

Fig. 2. The length of the hypertrophic zone is doubled in *Runx2*$^{HC/HC}$ mice. (A) Hindlimbs from 3-days old littermates were processed for histology. Representative images of the whole tibia stained with H&E are shown at 4x magnification. Double headed red arrows indicate the length of the hypertrophic zone and black arrows show the length of the ossified region. Scale bar: 100 µm. (B) Box regions are shown at 10x magnifications. Scale bar: 200 µm. (C) Length of the overall growth plate from the articular surface to the end of the hypertrophic zone, (D) length of the zone of chondrocyte hypertrophy (HZ), and (E) length of the ossified region was quantified from four different tibias (n = 4) obtained from *Runx2*$^{+/+}$ and *Runx2*$^{HC/HC}$ littermates. Data are presented in a scatter plot showing mean and SDM. (F) Growth plates from the enzymatically cleared hindlimbs of 3-days old *Runx2*$^{+/+}$ and *Runx2*$^{HC/HC}$ littermates (n = 5) were dissected, and flash frozen for RNA extraction. Relative expression of *Ihh*, *Col10a*, *Pthrp*, *Sox9*, and *Col2* genes normalized with *Gapdh* is presented in box and whisker plot. (*P < 0.05, **P < 0.01, ***P < 0.001). (For interpretation of the references to colour in this figure legend, the reader is referred to the web version of this article.)

To explore the molecular basis for changes in the growth plate, the expression of chondrocyte marker genes was assessed by qPCR analysis. Consistent with the enlarged hypertrophic zone, a 3.5 fold increase in expression of the pre-hypertrophic marker (*Ihh*) and hypertrophic chondrocyte marker (*Col10*) was noted in *Runx2*$^{HC/HC}$ littermates (Fig. 2F). Interestingly, *Pthrp*, which is expressed by resting chondrocytes, also showed a 2.5-fold increased expression in *Runx2*$^{HC/HC}$ mice (Fig. 2F). However, the mRNA levels of the essential chondrocyte transcription factor *Sox9* and the major collagen in the hyaline cartilage (*Col2*) are comparable among the littermates. (Fig. 2F). Thus, loss of the *Runx2* gene from hypertrophic chondrocyte results in significant changes in both the growth plate and the ossified zone, leading to limb dwarfism.

Runx2 promotes apoptosis of hypertrophic chondrocytes

The enlarged zone of hypertrophic chondrocytes in *Runx2*$^{HC/HC}$ mice could be due to an increase in chondrocyte proliferation and subsequent hypertrophic differentiation or a decrease in apoptosis of hypertrophic chondrocytes. To assess these possibilities, cell death and proliferation assays were performed. We evaluated apoptosis of chondrocytes in paraffin-embedded sections of the hindlimb. A significant reduction in TUNEL positive hypertrophic chondrocytes is noted in both the distal femur and proximal tibial growth plates of *Runx2*$^{HC/HC}$ littermates (Fig. 3A). Quantification of TUNEL positive hypertrophic chondrocytes revealed a 25% and 30% decrease in the femur and tibia growth plates respectively (Fig. 3B). To independently confirm changes in chondrocyte apoptosis, we monitored the expression of pro-apoptotic and anti-apoptotic genes in the epiphyseal region of the tibia and femur from 3-days old littermates. The expression of the pro-apoptotic *Bax* gene was drastically reduced in *Runx2*$^{HC/HC}$ mice. Quantification of *Bax* mRNA from five littermates showed an 81% decrease in the *Runx2*$^{HC/HC}$ mice (Fig. 3C). Interestingly, the expression levels of the anti-apoptotic *Bcl2* gene showed no significant difference among littermates (Fig. 3C). The ratio between the expression level of an anti-apoptotic and pro-apoptotic gene determines a cells resistance to apoptosis. The *Bcl2* to *Bax* ratio is increased by 4-fold in the *Runx2*$^{HC/HC}$ mice, indicating resistance to apoptosis (Fig. 3C). These results strongly suggest that RUNX2 regulates apoptosis of hypertrophic chondrocytes during endochondral ossification.

To test if chondrocyte proliferation contributes to an enlarged hypertrophic zone, the expression of proliferation marker genes was compared among littermates (Fig. 3D). *Runx2*$^{HC/HC}$ mice showed a

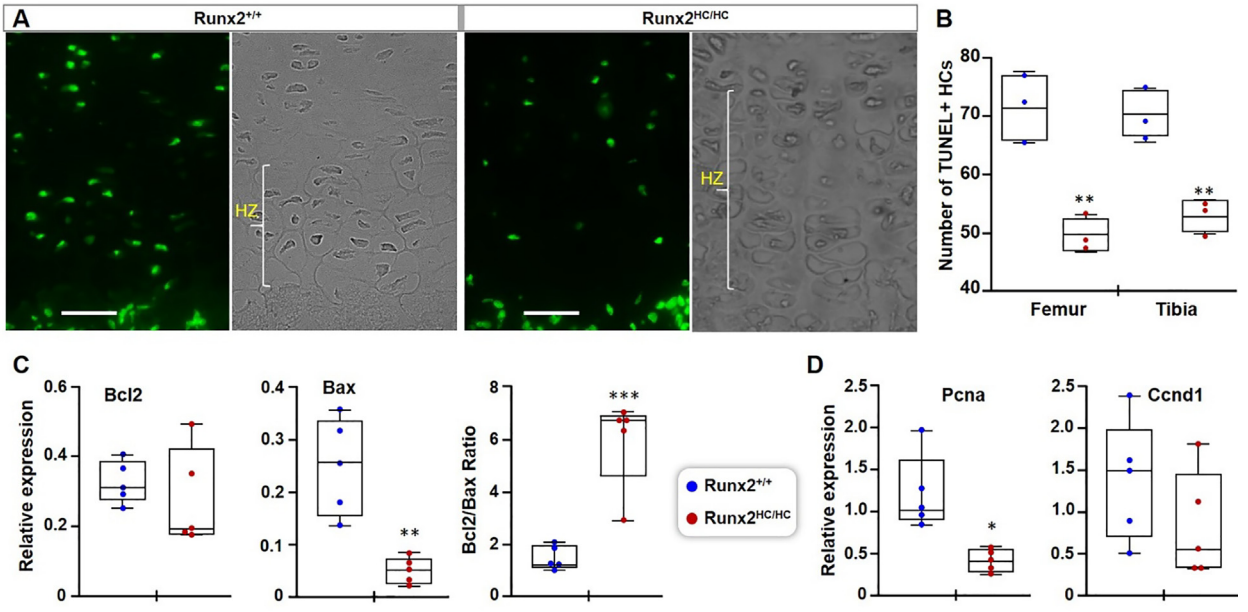

Fig. 3. Decrease apoptosis of hypertrophic chondrocytes contributes to the lengthening of the zone of hypertrophy. (A) Hindlimbs from 3-days old littermates were processed for histology. Representative images from tibial growth plates are shown at 40x magnification. Scale bar: 50 μm. (B) TUNEL positive hypertrophic chondrocytes counted from proximal and distal growth plates of tibia and femur from three littermates (n = 3) are presented in box and whisker plot. (C, D) Enzymatically cleared distal femur and proximal tibia epiphyseal growth plates from 3-days old *Runx2*$^{+/+}$ and *Runx2*$^{HC/HC}$ littermates (n = 5) were used for RNA extraction. Relative expression of (C) *Bax* and *Bcl2*, (D) *Pcna*, and *Ccnd1* genes normalized with *Gapdh* are shown in the box and whisker plot. (*$P < 0.05$, **$P < 0.01$, ***$P < 0.001$).

significant reduction in the expression of proliferating cell nuclear antigen (*Pcna*). However, expression of cyclin D1(*Ccnd1*), another marker of cell proliferation, showed no change among littermates (Fig. 3D). Taken together these data indicate that the lengthening of the zone of hypertrophy in *Runx2*$^{HC/HC}$ is likely due to a decrease in the apoptosis of hypertrophic chondrocytes.

Deletion of Runx2 in hypertrophic chondrocytes leads to impaired resorption of cartilage matrix

The decreased ossified region in the long bones of *Runx2*$^{HC/HC}$ mice prompted the assessment of the cartilage matrix in the developing limbs. Alcian blue stained tibia sections showed the presence of a significant amount of cartilage matrix in both the proximal and distal metaphysis region in *Runx2*$^{HC/HC}$ mice (Fig. 4A). The cartilage erosion zone is significantly expanded and the remnants of hypertrophic cartilage are present up to the mid-diaphysis region of the tibia (Fig. 4B). Quantification of hypertrophic cartilage length indicates a 56% increase in both the proximal and the distal growth plate of homozygous mice (Fig. 4C). A significant increase in the cartilage erosion zone is also noted in the femur of the *Runx2*$^{HC/HC}$ mice (data not shown). The cartilage accumulation in the mice may be due to an increased synthesis or decreased resorption of the cartilage matrix. To distinguish these possibilities, we analyzed the expression of the most abundant proteoglycan (*Acan*) and collagen (*Col2*) produced by chondrocytes. As noted earlier the expression of *Col2* is comparable among littermates (Fig. 2F). To our surprise, the expression of *Acan* is decreased by 20% in the *Runx2*$^{HC/HC}$ littermates (Fig. 4D). These results indicate that the increased amount of cartilage in the Runx2 mutant mice is not due to enhanced cartilage synthesis.

The turnover of the calcified cartilage in the developing limb is regulated by several matrix degrading enzymes primarily produced by hypertrophic chondrocytes. Therefore, we evaluated the expression of collagenase-3 (*Mmp13*), gelatinase-B (*Mmp9*), and aggrecanases (*Adamts4, Adamts5*) among littermates. Expression of both collagenase-3 and gelatinase-B is decreased by 65% in *Runx2*$^{HC/HC}$ compared to littermates (Fig. 4E). Expression of *Adamts4* and *Adamts5* was significantly decreased by 75% and 81% respectively in *Runx2*$^{HC/HC}$ littermates (Fig. 4E). We also examined gene expression of tissue inhibitors of metalloproteinases (*Timps*), that are known to

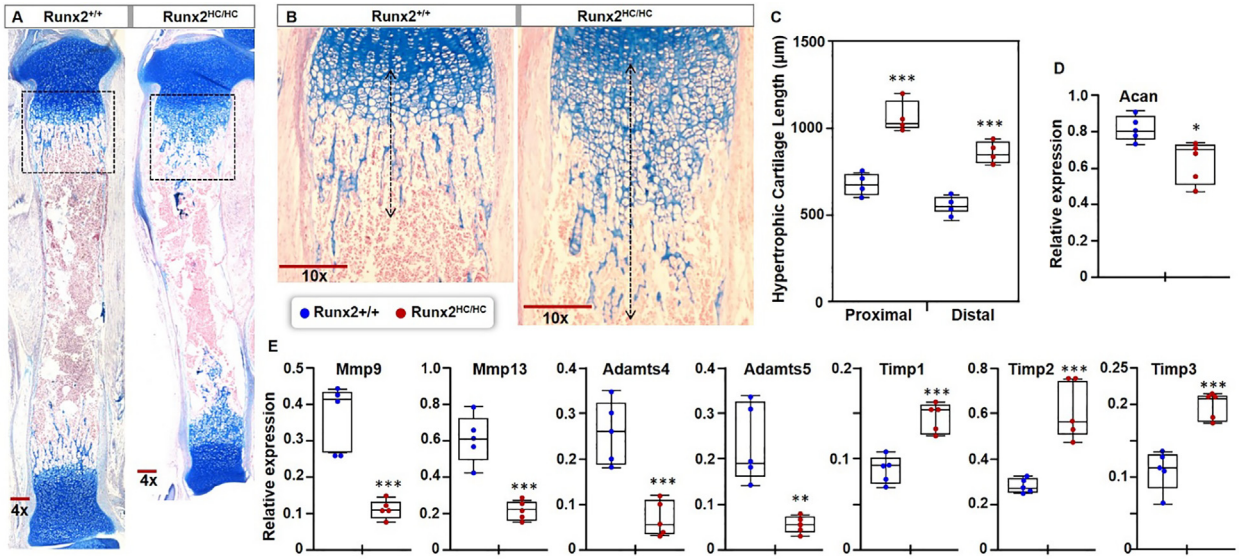

Fig. 4. Accumulation of hypertrophic cartilage in *Runx2*$^{HC/HC}$ mice is associated with decreased expression of matrix metalloproteinase. (A) Representative images of alcian blue stained whole tibia from 3-days old littermates. (B) The boxed region is shown at 10x magnification. Double headed arrows indicate the length of hypertrophic cartilage. Scale bar: 200 μm. (C) The length of hypertrophic cartilage measured from the start of the hypertrophic zone to the end of cartilage remnant in littermates (n = 4) is presented in a box and whisker plot. (D, E) RNA isolated from the enzymatically cleared distal femur and proximal tibia epiphyseal growth plates from *Runx2*$^{+/+}$ and *Runx2*$^{HC/HC}$ littermates (n = 5) subjected to qPCR. Relative expression of *Acan*, *Mmp9*, *Mmp13*, *Adamts4*, *Adamts5, Timp1, Timp2 and Timp3* normalized with *Gapdh* is shown in the box and whisker plot. (*$P < 0.05$, **$P < 0.01$, ***$P < 0.001$). (For interpretation of the references to colour in this figure legend, the reader is referred to the web version of this article.)

regulate the activity of collagenases and aggrecanases. Interestingly, expression of *Timp1*, *Timp2* and *Timp3* was increased by 65%, 120% and 80% respectively in *Runx2*$^{HC/HC}$ littermates. These results suggests that cartilage accumulation is likely linked with the decreased expression and activity of cartilage degrading enzymes. Together our data indicate that RUNX2 activity in hypertrophic chondrocytes is required for the expression of the enzymes responsible for the degradation of the calcified cartilage matrix.

Increased calcified cartilage in Runx2$^{HC/HC}$ mice is associated with a decrease in the number of chondroclasts

In addition to the matrix degrading enzymes secreted by hypertrophic chondrocytes, turnover of the hypertrophic cartilage is regulated by chondroclasts. TRAP staining of the tibial section showed a marked decrease in the number of TRAP positive cells in the cartilage erosion zone of *Runx2*$^{HC/HC}$ littermates (Fig. 5A). To better quantify the difference in cartilage resorbing cells, the paraffin sections from hindlimb were double stained with TRAP and alcian blue. Consistent with the earlier observation, *Runx2*$^{HC/HC}$ bones showed a significant decrease in the number of TRAP + chondroclasts lining the cartilage island within the erosion zone (Fig. 5B). Quantification from five littermates revealed a 35% decrease in the number of TRAP + chondroclast in *Runx2*$^{HC/HC}$ mice (Fig. 5C). Next, we performed qPCR analysis to evaluate the expression of genes regulating the differentiation of chondroclasts. Interestingly, expression of *Rankl* is decreased by 73% in the growth plate chondrocyte of *Runx2*$^{HC/HC}$ mice. In sharp contrast expression of *Opg* is increased by 75% in the *Runx2*$^{HC/HC}$ littermates. This differential gene expression in the *Runx2*$^{HC/HC}$ mice resulted in a decreased ratio of *Rankl*/*Opg*, which is inhibitory for chondroclast differentiation (Fig. 5D). Together our results suggest that *Runx2* deficiency in the hypertrophic chondrocytes leads to impaired differentiation of chondroclasts and cartilage resorption in the developing bones.

Runx2$^{HC/HC}$ mice exhibits increased trabecular bone mass

During endochondral ossification, hypertrophic cartilage provides the template for bone synthesis. Therefore, we performed Von Kossa staining to assess if an increased amount of hypertrophic cartilage in *Runx2*$^{HC/HC}$ mice affects mineral

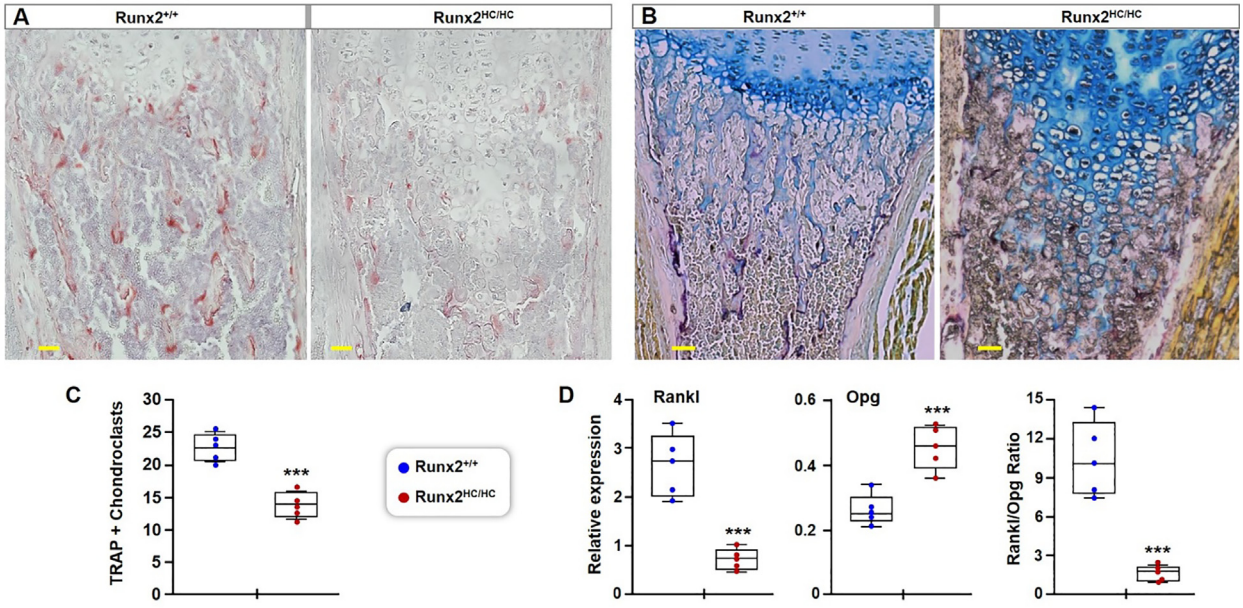

Fig. 5. *Runx2*$^{HC/HC}$ mice show a decreased number of TRAP positive chondroclasts in the cartilage erosion zone. (A) Hindlimbs from 3-days old littermates were processed for histology and stained with TRAP. A representative image of TRAP-stained tibia from *Runx2*$^{+/+}$ and *Runx2*$^{HC/HC}$ littermates is shown at 10x magnification. (B) TRAP and alcian blue double staining performed to reveal the cartilage associated with TRAP + chondroclasts. Representative images are presented at 10x magnification. Scale bar: 100 μm. (C) The number of TRAP + chondroclasts counted from five littermates (n = 5) is presented in a box and whisker plot. (D) RNA isolated from enzymatically cleared epiphyseal growth plates from indicated littermates was used for qPCR performed with four replicates. Relative *Opg* and *Rankl* expression normalized with *Gapdh* is shown in the box and whisker plot. The calculated *Rankl*/*Opg* ratio for each sample is presented in a box and whisker plot. (***$P < 0.001$). (For interpretation of the references to colour in this figure legend, the reader is referred to the web version of this article.)

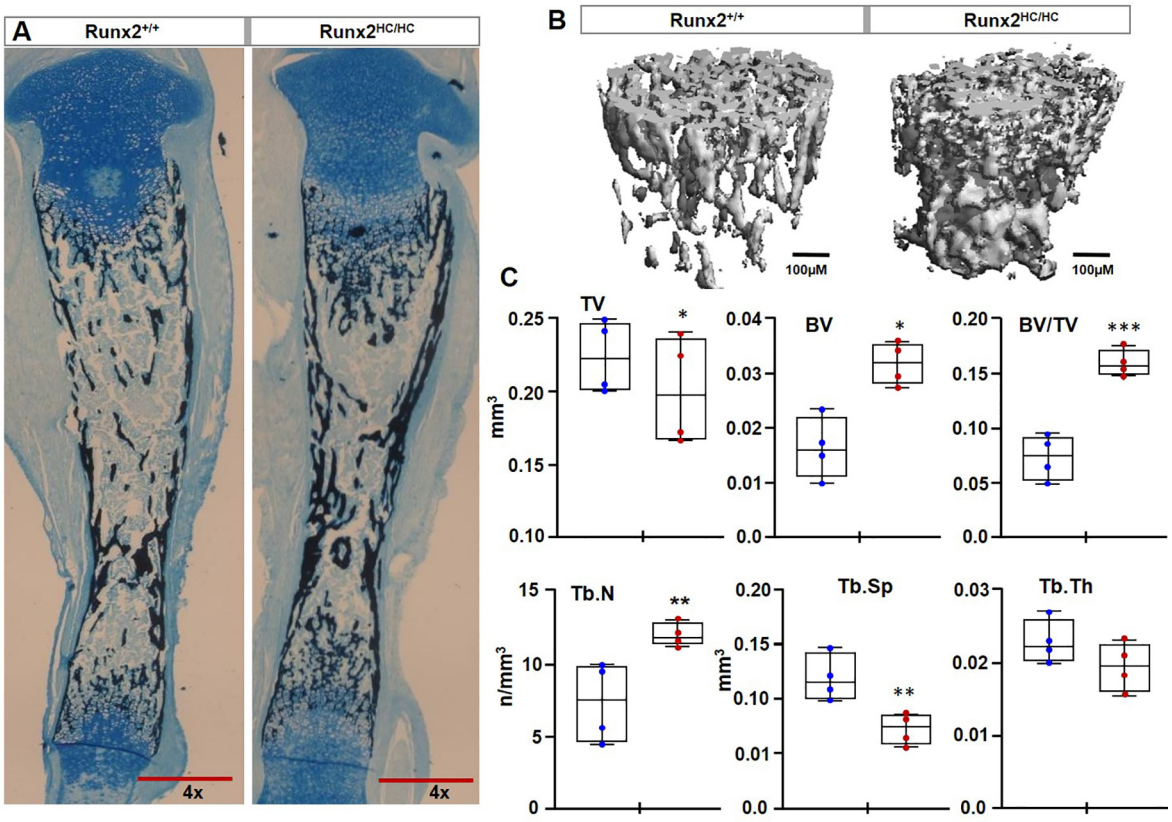

Fig. 6. Increased trabecular mineralization in *Runx2* mutant mice. (A) Paraffin sections of the tibia from 3-days old littermates were stained with Von Kossa followed by alcian blue. Representative images of the tibia taken at 4x magnification are shown. Scale bar: 500 μm. (B) Representative 3D-image of trabecular bone from the femur of 3-days old *Runx2*$^{+/+}$ and *Runx2*$^{HC/HC}$ littermates. Scale bar: 100 μm. (C) Trabecular bone parameters were analyzed from a 2.4 mm region immediately beneath the growth plate. Quantified data of bone parameters from *Runx2*$^{+/+}$ and *Runx2*$^{HC/HC}$ littermates (n = 4) is presented in a box and whisker plot. BV; bone volume, TV; total volume, Tb.N; trabecular number, Tb.Th; trabecular thickness, Tb.Sp; trabecular space. (*$P < 0.05$, **$P < 0.01$, ***$P < 0.001$). (For interpretation of the references to colour in this figure legend, the reader is referred to the web version of this article.)

deposition. A marked increase in mineral deposition was evident at both the proximal and distal growth plates of the tibia of *Runx2*$^{HC/HC}$ littermates (Fig. 6A). Hindlimbs used to evaluate bone mass by micro-CT analysis confirmed an increase in trabecular bone (Fig. 6B). Quantification from four littermates showed a 2-fold increase in the BV/TV ratio of the trabecular bone in *Runx2*$^{HC/HC}$ mice (Fig. 6C). Importantly, a 50% increase in the trabecular number was coupled with a 30% decrease in trabecular spacing in *Runx2*$^{HC/HC}$ mice (Fig. 6C). The trabecular thickness and bone surface, however, remain unchanged among littermates (Fig. 6C and data not shown). The cortical bone was comparable among littermates and bone parameters determined at the mid-diaphysis region such as BV/TV, cortical thickness, bone surface and porosity were comparable between *Runx2*$^{+/+}$ and *Runx2*$^{HC/HC}$ littermates (data not shown). Together our data demonstrate that increase mineral deposition in the trabecular bone is associated with retention of hypertrophic cartilage.

Discussion

In the current study, the *Runx2* gene is deleted in hypertrophic chondrocytes to assess its physiologic role after chondrocyte hypertrophy. Homozygous mice have comparable body weights and survive to adulthood. *Runx2*$^{HC/HC}$ mice exhibit limb dwarfism and unmineralized metacarpals and metatarsals. *Runx2* gene ablation in the hypertrophic chondrocyte does not affect the resting or proliferative zone in the growth plate but the zone of chondrocyte hypertrophy is nearly doubled. The expansion of the hypertrophic zone in growth plates is mainly due to a significant reduction in apoptosis of the hypertrophic chondrocytes. Decreased expression of the matrix degrading enzymes by *Runx2*-deficient hypertrophic chondrocytes leads to accumulation of calcified cartilage in the limb bones. Moreover, *Runx2*$^{HC/HC}$ mice showed a significant reduction in TRAP + chondroclasts and an increase in trabecular bone mass. Thus, RUNX2 continues to function after chondrocyte hypertrophy to control

the turnover of hypertrophic cartilage during endochondral ossification.

Impairments in the chondrocyte differentiation and endochondral ossification process are central to the dwarfism phenotype. *Runx2*$^{HC/HC}$ mice have shorter limbs and a decreased length of the ossified region. The reason for the shortening of the long bone could be a decrease in the proliferation of chondrocytes. IHH produced by hypertrophic chondrocyte regulates chondrocyte proliferation by inducing expression of *Pthrp* in the resting chondrocyte [46]. Deletion of either *Ihh* or *Pthrp*, therefore, leads to proliferative defects and dwarfism [15,47]. RUNX2 directly regulates the expression of both *Ihh* and *Pthrp* [17,48,49]. Deletion of *Runx2* in resting chondrocytes and the resultant decrease in *Ihh* expression and chondrocyte proliferation leads to dwarfism [17]. However, *Runx2* deletion in hypertrophic chondrocyte did not show any change in chondrocyte proliferation as the length of the proliferative zone and *Ccnd1* expression were comparable among wild-type and homozygous littermates. Our data are consistent with the recent report showing no change in chondrocyte proliferation upon deletion of the *Runx2* gene in hypertrophic chondrocytes [50]. The increased levels of *Ihh* and *Pthrp* noted in *Runx2*$^{HC/HC}$ mice likely reflect an increase in the number of the pre-hypertrophic/hypertrophic chondrocytes within the enlarged growth plate. These results indicate that dwarfism in *Runx2*$^{HC/HC}$ mice is not due to chondrocyte proliferation.

A surprising finding in our study is the doubling of the zone of hypertrophic chondrocytes in *Runx2*$^{HC/HC}$ littermates. Accelerated maturation or decreased apoptosis of hypertrophic chondrocytes can lead to the lengthening of the hypertrophic zone. For example, activation of β-catenin signaling in resting chondrocytes leads to a significant expansion of the hypertrophic zone due to accelerated maturation and shortened proliferative zone, but without affecting chondrocyte apoptosis [51]. Our histological analysis reveals that the overall length of the growth plate is significantly increased but the length of the resting and proliferating zone is comparable among wild-type and homozygous littermates. Moreover, the expression of the proliferative marker is either unchanged (*Ccnd1*) or significantly decreased (*Pcna*) in *Runx2*$^{HC/HC}$ mice. Our results are consistent with no change in proliferation demonstrated by BrdU labeling in mice where the *Runx2* gene is deleted in hypertrophic chondrocytes [50]. Thus, the accelerated maturation is unlikely a contributing factor for the doubling of the zone of chondrocyte hypertrophy in *Runx2*$^{HC/HC}$ mice.

A significant decrease in apoptosis of hypertrophic chondrocytes is associated with enlargement of the zone of hypertrophy [26]. BCL2 and BAX proteins promote cell survival and apoptosis, respectively. Expression of the anti-apoptotic *Bcl2* gene is highest in the proliferative chondrocytes but is nearly absent in hypertrophic chondrocytes [52]. Deletion of the *Bcl2* gene results in the shortened hypertrophic zone due to increased apoptosis of hypertrophic chondrocytes [52]. In sharp contrast, expression of the pro-apoptotic BAX protein increases progressively during chondrocyte differentiation with the maximum levels noted in hypertrophic chondrocyte [52]. Deletion of the *Bax* gene results in decreased apoptosis of chondrocytes [53]. In line with the decreased apoptosis of hypertrophic chondrocytes in *Runx2*$^{HC/HC}$ mice, our qPCR analysis showed no change in *Bcl2* mRNA but a significant decrease in the expression of the *Bax* gene. This differential expression leads to a 4-fold increase in the *Bcl2*/*Bax* ratio, which normally inhibits cellular apoptosis. Therefore, the expansion of the hypertrophic zone in *Runx2*$^{HC/HC}$ mice is likely due to a decrease in apoptosis of hypertrophic chondrocytes. Importantly, Runx2 binds and regulates the activity of *Bcl2* and *Bax* promoters [54,55]. In stark contrast to our data, a recent report shows that *Runx2* deletion in hypertrophic chondrocytes promotes apoptosis of hypertrophic chondrocytes without changing the length of the hypertrophic zone. Surprisingly, increase apoptosis of hypertrophic chondrocytes was noted despite no change in the expression of the pro-apoptotic *Bax* gene and a significant increase in the mRNA of the anti-apoptotic *Bcl2* gene [50]. The underlying reasons for these contrasting findings need further investigation.

During endochondral ossification, degradation of cartilage and formation of bone are coupled. Compared to wild-type littermates, a large amount of calcified cartilage was present in the *Runx2*$^{HC/HC}$ mice. The cartilage islands were noted well beyond the metaphyseal regions of the endochondral bones. The production of ACAN and COL2 mainly determines the amount of cartilage matrix in the developing endochondral bones [56,57]. A similar expression level of *Acan* and *Col2* mRNA among littermates rules out that increased cartilage synthesis is contributing to the accumulation of cartilage matrix in *Runx2*$^{HC/HC}$ mice. Enzymes produced by hypertrophic chondrocytes such as aggrecanase, gelatinase, and collagenase are critical for the degradation of the calcified cartilage [58]. Deletion of gelatinase (*Mmp9*) or collagenase (*Mmp13*) genes in mice disrupts cartilage degradation, leading to accumulation of hypertrophic cartilage in the long bone [26,27]. In humans, a mutation in the gelatinase or collagenase genes results in metaphyseal dysplasia characterized by defective growth and modeling of the spine and long bones [59,60].

ADAMTS4 and ADAMTS5 are the major aggrecanase involved in degradation of aggrecan [61]. Global deletion of *Adamts4* or *Adamts5* gene in mice does not impair embryonic skeletogenesis [62,63]. However, *Adamts5* is required for development of trabeculated bone in the mandibular condyle

[64]. Interestingly, *Adamts5* deficiency prevents cartilage degradation in both inflammatory and surgically induced murine model of osteoarthritis [62,63]. In humans, single nucleotide polymorphism in *ADAMTS5* gene is associated with lumbar degenerative disc disease [65]. It is important to note that RUNX2 directly regulates the expression of gelatinase, collagenase, and aggrecanase [66–69]. We find *Runx2* deletion in hypertrophic chondrocytes results in a significant reduction in expression of *Adamts4*, *Adamts5*, *Mmp9*, and *Mmp13*. The reported decrease in Mmp13 expression due to deletion of Runx2 in hypertrophic chondrocytes at the embryonic stage is consistent with our data, but expression of *Mmp9*, *Adamts4* or *Adamts5* is not described in this paper [47]. Thus, RUNX2 activity in hypertrophic chondrocytes is required to produce enzymes that are responsible for the degradation of the calcified cartilage.

During development, the four members of the tissue inhibitors of metalloproteinases gene family (*Timp1-4*), are ubiquitously expressed in several tissues and cancers [70]. TIMPs inhibits activity of MMPs and ADAMTSs by forming an irreversible complex with the enzyme in a 1:1 ratio [71]. During cartilage development, *Timp1*, *Timp2* and *Timp3* are expressed by chondrocytes [28–31]. Due to the redundant functions, no skeletal phenotype is noted when *Timp* genes are individually deleted in mice [72]. However, combined deletion of *Timp*1-4 leads to enhanced degradation of cartilage and significant shortening of long bones [72]. The proximal promoters of *Timp*1, 2 and 3 contain a Runx binding motif and RUNX2 overexpression induce activity of *Timp*1 promoter in fibroblasts [73,74]. We noted a significant increase in expression of *Timp1, Timp2* and *Timp3* in $Runx2^{HC/HC}$ mice. Therefore, the accumulation of hypertrophic cartilage in $Runx2^{HC/HC}$ mice is likely due to a decrease in expression and activity of cartilage degrading enzymes.

Another surprising finding of our study is the significant increase of trabecular bone mass in $Runx2^{HC/HC}$ mice. The high bone mass is not due to increased bone synthesis, as the expression of osteoblast markers such as collagen type I and osteocalcin are comparable among the littermates (unreported observation). Chondroclasts are essential for the turnover of hypertrophic cartilage, which serves as a template for mineral deposition during endochondral ossification. A 35% decrease in the number of chondroclasts noted in the cartilage erosion zone/trabecular bone region of the $Runx2^{HC/HC}$ mice is likely responsible for the retention of hypertrophic cartilage. Hypertrophic chondrocytes produced RANKL and OPG is central for the differentiation of chondroclasts/osteoclasts [33,75]. During endochondral ossification, RUNX2 regulates the expression of both *Rankl* and *Opg* in chondrocytes and the *Rankl*/*Opg* ratio is critical for chondroclast/osteoclast differentiation [76,77]. We find a significant increase in *Opg* mRNA and a significant decrease of *Rankl* expression in $Runx2^{HC/HC}$ mice. This differential expression leads to 81% decrease in the *Rankl*/*Opg* ratio, which is inhibitory for chondroclast/osteoclast differentiation. We have previously reported that deletion of the *Runx2* gene in resting chondrocytes blocks chondrocyte hypertrophy, decreases expression of *Rankl*/*Opg* and results in an absence of TRAP + c hondroclasts [17]. Together, our results demonstrate RUNX2 controlled *Rankl* and *Opg* expression in hypertrophic chondrocytes is required for chondroclast/osteoclast differentiation. In contrast to our finding, a significant increase in the number of TRAP + osteoclasts is reported in E16.5 *Runx2* homozygous null mice but without any change in the *Rankl*/*Opg* ratio. Interestingly, a significant decrease in the *Rankl*/*Opg* ratio is noted a day earlier in this model but neither the TRAP staining nor the quantification of TRAP + osteoclast is presented at E15.5 [50]. Further investigation is needed to reconcile the discrepancies in the cartilage and trabecular bone phenotype between the two *Runx2* mouse models.

Conclusion

In conclusion, our findings uncover a novel role of RUNX2 in regulating apoptosis of hypertrophic chondrocytes and degradation of cartilage matrix during endochondral ossification. Regulation of *Rankl* and *Opg* expression by RUNX2 in hypertrophic chondrocytes is critical for chondroclast/osteoclast differentiation and resorption of cartilage and bone matrix.

Experimental procedures

Generation and genotyping of $Runx2^{HC/HC}$ mouse

Generation of exon 8 Runx2-floxed ($Runx2^{F/F}$) mice is reported previously [17]. To delete Runx2 specifically in hypertrophic chondrocytes, $Runx2^{F/F}$ mice were crossed with BAC-collagen type10-Cre mice [45]. The resulting heterozygous ($Runx2^{+/HC}$) mice were intercrossed to obtain $Runx2^{HC/HC}$, $Runx2^{+/HC}$, and $Runx2^{+/+}$ mice. The Ai9-tdTomato reporter mouse was used to confirm the specificity of Cre-expression [78]. All genotypes were determined using DNA from the tail biopsy with Direct PCR lysis reagent (Viagen biotech, Cat#102-T). The Runx2 wild type and floxed alleles, ROSA26-Tdtomato and Cre transgene were detected by PCR using the specific primers in Table 1. All animal experiments were performed with the approval of the Institutional Animal Care and Use Committee of the University of Alabama at Birmingham and conformed to relevant federal and state guidelines and regulations.

Table 1 Primer sequence used for genotyping of mice.

Name	Forward (5′ to 3′)	Reverse (5′ to 3′)
Runx2	atc agt tcc caa tgg tac ccg	gca aga tca tga cta ggg att g
Col10-Cre	ttt aga gca tta ttt caa ggc agt ttc	agg caa att ttg gtg tac gg
tdTomato	ctg ttc ctg tac ggc atg g	ggc att aaa gca gcg tat cc

Skeletal staining and histology

For skeletal staining with alizarin red and alcian blue, littermates of all genotypes were collected at 3-days of age. We follow previously published protocol for staining of newborn pups with some modification [17]. Hindlimbs and forelimbs were dissected and de-skinned, and muscles were partially removed. Limbs were fixed for 3 days in 95% ethanol (EtOH) and then placed in acetone for 2 days to remove fat tissues. Skeletons were then placed in alizarin red and alcian blue staining solution 0.015% alcian blue (Sigma-Aldrich, Cat#A5268), 0.005% alizarin red (MP Biomedicals, Cat# 100375), and 5% Acetic acid in 70% ethanol for 3 days with gentle shaking. The soft tissues from the stained skeleton were cleared with 0.5% KOH for 2 days with gentle shaking and the fresh solution was used every day. The further clearing was carried out with 0.5% KOH and sequential concentrations of glycerol (20%, 50%, and 80%) for 3 days for each with gentle shaking. Stained skeleton preparations were stored in 0.5% KOH and 80% glycerol for complete cleaning. Skeletal elements of both WT and *Runx2*$^{HC/HC}$ were captured in the same frame with Nikon Cool PIX S10 digital camera (Nikon, Cat#2555B).

Tissue embedding for histological sectioning and staining was performed essentially as previously published [17,79]. For histological analysis, hindlimbs from 3-days old littermates were fixed overnight in 4% paraformaldehyde (Sigma-Aldrich, Cat#P6148). Tibia and femur were dehydrated in gradient ethanol, embedded in paraffin, and sectioned at 7 μm thickness. Tissue sections were dewaxed in xylene, rehydrated in gradient ethanol, and processed for hematoxylin and eosin, alcian blue, and TRAP staining as described elsewhere [79].

TRAP and alcian blue double staining

The tissue sections were double stained with TRAP and alcian blue to reveal the cartilage associated chondroclasts. TRAP staining was performed by incubating slides in the naphthol AS-BI phosphate solution for 2 hrs at room temperature using acid phosphatase leucocyte kit (Sigma-Aldrich, Cat#387A). The slides were washed in PBS for 5 min and then stained with 0.2% alcian blue solution in 3% acetic acid. The slides were washed with three changes of water for 5 min each.

Micro-CT analysis

Trabecular and cortical bone structure and mineral density were analyzed in 3-days old mice by μCT analysis with the help of UAB Small Animal Imaging and Analysis Core. Undecalcified femurs were scanned by a cone beam microcomputed tomography system μCT40 to produce 3D images (Scanco Medical AG, Brüttisellen, Switzerland). Images were analyzed using μCT 3D Viewer V3.8 software. Quantification of bone parameters for cortical bone were derived from a 0.6 mm region of the femoral mid-shaft and trabecular bone from a 2.4 mm region immediately beneath the growth plate. Bone parameters analyzed were; bone volume (BV), total volume (TV), trabecular number (Tb.N), trabecular thickness (Tb.Th), and trabecular space (Tb.Sp).

RNA isolation and quantitative real time PCR

Analysis of the gene expression by qPCR was performed as previously published [80]. Briefly, total RNA was extracted from the distal femur and proximal tibia of hindlimbs of 3-days old littermates. De-skinned hindlimbs were completely cleared of skeletal muscle by digestion initially with pronase (Roche Diagnostic, Cat#10165921001) and collagenase-D (Roche Diagnostic, Cat#11088882001) for 1-hr and subsequently with collagenase-D for 2 hrs at 37 °C. The epiphysial growth plates were harvested under dissecting microscope and flash frozen in liquid nitrogen and homogenized in PBS containing DEPC. The growth plate homogenates were sonicated in TRIZOL reagent (Life Technologies, Cat# 15596018) to extract total RNA. The cDNA was prepared from 1.5 μg of total RNA using a cDNA synthesis kit (BioRad, Cat# 170-8891). Quantitative real time PCR with four replicates was performed using iQ SYBR Green Supermix (BioRad, Cat# 1725124) with specific primer pairs detailed in Table 2. Gene expression values were normalized with Gapdh, used as an internal control. Relative gene expression was obtained using the 2^-$^{\Delta CT}$ method.

TUNEL assay

Terminal deoxynucleotidyltransferase-mediated dUTP-biotin nick end labeling (TUNEL) staining was performed using fluorescein *in situ* cell death detection kit (Roche Applied Science, Cat# 11684795910). Paraffin sections from hindlimbs of

Table 2 Sequence of primers used for qPCR.

Name	Forward (5′ to 3′)	Reverse (5′ to 3′)
Acan	ccc tcc ggc aga aga aag at	cgc ttc tgt agc ctg tgc ttg
Col2	tcc tct gcg atg aca tta tct	gat cat ctc tgg gtc ctt gtt
Sox9	agg aag ctg gca gac cag ta	tgt aat cgg ggt ggt ctt tc
Col10a	gca gca tta cga ccca aag at	ctt gaa gcc tga tcc agg ta
Ihh	acg tgc att gct ctg tca ag	ctc gat gac ctg gaa agc tc
Pthrp	ttc agc agt gga gtg tcc tg	agc tct gat ttc ggc tgt gt
Adamts4	caa gca gtc ggg ctc ctt	gatcgtgaccacatcgctgta
Adamts5	cca gtt gta caa aga tta tcg gaa cct	gtt gct cct tca ggg atc ct
Mmp9	gat ccc cag agc gtc att	cca cct tgt tca cct cat tt
Mmp13	tgt ttg cag agc act act tga a	cag tca cct cta agc caa aga aa
Bax	tgc aga gga tga ttg ctg ac	gat cag ctc ggg cac ttt ag
Bcl2	ctg gca tct tct cct tcc ag	gac ggt agc gac gag aga ag
Cyclin d1	gcg tac cct gac acc aat ctc	ctc ctc ttc gca ctt ctg ctc
Pcna	ttt gag gca cgc ctg atc c	gga gacgtg aga cga gtc cat
Rankl	act tgg gat ttt gat gct ggt t	tgg gcc aag atc tct aac atg a
Opg	atg aac aag tgg ctg tg	cct cac tgt gca gtg ctg tt
Timp1	agg tgg tct cgt tga ttt ct	gta agg cct gta gct gtg cc
Timp2	gaa tcc tct tga tgg ggt tg	cgt ttt gca atg cag acg ta
Timp3	ctt ctg caa ctc cga cat cgt	ggg gca tct tac tga agc ctc
Gapdh	ccg cct gga gaa acc tgc caa g	gga tag ggc ctc tct tgc tca g

3-day old littermates were processed for TUNEL labeling according to the manufacturer's directions. The tissue was permeabilized with 0.1% Triton-X 100 in 0.1% sodium citrate for 20 min at room temperature. Slides were placed in PBS for 10 mins and the TUNEL labeling reaction carried for 1.5 hrs at room temperature. Slides were washed twice with PBS for 10 mins each prior to mounting. Images of growth plate were captured using BZ-X8000 Keyence Fluorescence microscope. TUNEL positive nuclei within hypertrophic chondrocyte zone from both distal femur and proximal tibia were quantified.

Statistical analysis

Mean values and standard deviation of the means (SDM) were calculated using GraphPad Prism 9.0.0. Statistical significance was determined between $Runx2^{+/+}$ and $Runx2^{HC/HC}$ using an unpaired Student's *t* test. Data with $P < 0.05$ were considered statistically significant and are indicated with an asterisk in the figures. Data are presented either in a Scatter plot or a Box-whisker plot showing maximum to minimum values, mean, and SDM.

CRediT authorship contribution statement

Harunur Rashid: Conceptualized the experiments, Data curation, Validation, Visualization, Performed formal analysis, Funding acquisition, Writing of the original draft, Review and editing. **Haiyan Chen:** Conceptualized the experiments, Data curation, Validation, Visualization. **Amjad Javed:** Conceptualized the experiments, Performed formal analysis, Funding acquisition, Writing of the original draft, Review and editing.

DECLARATION OF COMPETING INTEREST

The authors declare that they have no known competing financial interests or personal relationships that could have appeared to influence the work reported in this paper.

Acknowledgements

Research reported in this publication was supported by the National Institute of Arthritis and Musculoskeletal and Skin Diseases, and National Institute on Aging of the National Institutes of Health under Award Number R01AR062091 and R56AG065129. H.R was supported by NIDCR training grant number, T-90DE022736, and a pilot grant from UAB GC-CODED. The content is solely the responsibility of the authors and does not necessarily represent the official views of the National Institutes of Health.

Author contribution

H.R, H.C and A.J outlined and designed experiments. H.R and H.C performed most of the

experiments. H.R and A.J performed analysis, interpretation of data and writing of the manuscript.

Received 26 April 2021;
Accepted 18 October 2021;
Available online 22 October 2021

Keywords:
Dwarfism;
Apoptosis;
Chondroclast/osteoclast;
Matrix-metalloproteinase;
Aggrecanase

Abbreviations:
SOX9, SRY box transcription factor; RUNX2, Runt related transcription factor 2; PTHRP, Parathyroid hormone-related peptide; ACAN, Aggrecan; COL2, Collagen type II; IHH, Indian hedgehog; COL10, Collagen type X; MMP, Matrix metalloproteinase; VEGFA, Vascular endothelial growth factor a; BAC, Bacterial artificial chromosome; CDK1, Cyclin-dependent kinase 1; RANKL, Receptor activator of nuclear factor Kappa B ligand; OPG, Osteoprotegerin; Wnt/PCP, Wnt/planar cell polarity; PCNA, Proliferating cell nuclear antigen; CCND1, Cyclin D1; TRAP, Tartrate-resistant acid phosphatase; TNAP, Tissue-nonspecific alkaline phosphatase

References

[1] Berendsen, A.D., Olsen, B.R., (2015). Bone development. *Bone*, **80**, 14–18.
[2] Akiyama, H., Chaboissier, M.C., Martin, J.F., Schedl, A., de Crombrugghe, B., (2002). The transcription factor Sox9 has essential roles in successive steps of the chondrocyte differentiation pathway and is required for expression of Sox5 and Sox6. *Genes Dev.*, **6** (21), 2813–2828.
[3] de Crombrugghe, B., Lefebvre, V., Behringer, R.R., Bi, W., Murakami, S., Huang, W., (2000). Transcriptional mechanisms of chondrocyte differentiation. *Matrix Biol.*, **19** (5), 389–394.
[4] Kronenberg, H.M., (2003). Developmental regulation of the growth plate. *Nature*, **423** (6937), 332–336.
[5] F. Long, D.M. Ornitz, Development of the endochondral skeleton, Cold Spring Harb Perspect Biol 5 (2013) a008334.
[6] Kozhemyakina, E., Lassar, A.B., Zelzer, E., (2015). A pathway to bone: signalingmolecules and transcription factors involved in chondrocyte development and maturation. *Development*, **142**, 817–831.
[7] Hallett, S.A., Ono, W., Ono, N., (2019). Growth plate chondrocytes: skeletal development, growth and beyond. *Int. J. Mol. Sci.*, **20**, 6009.
[8] Hojo, H., McMahon, A.P., Ohba, S., (2016). An emerging regulatory landscape for skeletal development. *Trends Genet.*, **32** (12), 774–787.
[9] Han, Y., Lefebvre, V., (2008). L-Sox5 and Sox6 drive expression of the aggrecan gene in cartilage by securing binding of Sox9 to a far-upstream enhancer. *Mol. Cell. Biol.*, **28** (16), 4999–5013.
[10] Mizuhashi, K., Ono, W., Matsushita, Y., Sakagami, N., Takahashi, A., Saunders, T.L., Nagasawa, T., Kronenberg, Ono, N., (2018). Resting zone of the growth plate houses a unique class of skeletal stem cells. *Nature*, **563** (7730), 254–258.
[11] Zhao, Q.i., Eberspaecher, H., Lefebvre, V., de Crombrugghe, B., (1997). Parallel expression of Sox9 and Col2a1 in cells undergoing chondrogenesis. *Dev. Dyn.*, **209** (4), 377–386.
[12] Saito, M., Mulati, M., Talib, S.Z., Kaldis, P., Takeda, S., Okawa, A., Inose, H., (2016). The indispensable role of cyclin-dependent kinase 1 in skeletal development. *Sci. Rep.*, **6**, 20622.
[13] Kato, K., Bhattaram, P., Penzo-Méndez, A., Gadi, A., Lefebvre, V., (2015). SOXC transcription factors induce cartilage growth plate formation in mouse embryos by promoting noncanonical Wnt signaling. *J. Bone Miner. Res.*, **30** (9), 1560–1571.
[14] Wyngaarden, L.A., Vogeli, K.M., Ciruna, B.G., Wells, M., Hadjantonakis, A.K., Hopyan, S., (2010). Oriented cell motility and division underlie early limb bud morphogenesis. *Development*, **137** (15), 2551–2558.
[15] St-Jacques, B., Hammerschmidt, M., McMahon, A.P., (1999). Indian hedgehog signaling regulates proliferation and differentiation of chondrocytes and is essential for bone formation. *Genes Dev.*, **13** (16), 2072–2086.
[16] van der Eerden, B.C., Karperien, M., Gevers, E.F., Löwik, C.W., Wit, J.M., (2000). Expression of Indian hedgehog, parathyroid hormone-related protein, and their receptors in the postnatal growth plate of the rat: evidence for a locally acting growth restraining feedback loop after birth. *J. Bone Miner. Res.*, **15** (6), 1045–1055.
[17] Chen, H., Ghori-Javed, F.Y., Rashid, H., Adhami, M.D., Serra, R., Gutierrez, S.E., Javed, A., (2014). Runx2 regulates endochondral ossification through control of chondrocyte proliferation and differentiation. *J. Bone Miner. Res.*, **29** (12), 2653–2665.
[18] Zelzer, E., Mamluk, R., Ferrara, N., Johnson, R.S., Schipani, E., Olsen, B.R., (2004). VEGFA is necessary for chondrocyte survival during bone development. *Development*, **131** (9), 2161–2171.
[19] Inada, M., Wang, Y., Byrne, M.H., Rahman, M.U., Miyaura, C., Lopez-Otin, C., Krane, S.M., (2004). Critical roles for collagenase-3 (Mmp13) in development of growth plate cartilage and in endochondral ossification. *PNAS*, **101** (49), 17192–17197.
[20] Retting, K.N., Song, B., Yoon, B.S., Lyons, K.M., (2009). BMP canonical Smad signaling through Smad1 and Smad5 is required for endochondral bone formation. *Development*, **136** (7), 1093–1104.
[21] Hill, T.P., Später, D., Taketo, M.M., Birchmeier, W., Hartmann, C., (2005). Canonical Wnt/beta-catenin signaling prevents osteoblasts from differentiating into chondrocytes. *Dev. Cell*, **8** (5), 727–738.
[22] Naski, M.C., Colvin, J.S., Coffin, J.D., Ornitz, D.M., (1998). Repression of hedgehog signaling and BMP4 expression in growth plate cartilage by fibroblast growth factor receptor 3. *Development*, **125** (24), 4977–4988.
[23] Hilton, M.J., Tu, X., Wu, X., Bai, S., Zhao, H., Kobayashi, T., Kronenberg, H.M., Teitelbaum, S.L., Ross, F.P., Kopan, R., Long, F., (2008). Notch signaling maintains bone marrow mesenchymal progenitors by suppressing osteoblast differentiation. *Nat. Med.*, **14** (3), 306–314.
[24] Schipani, E., Ryan, H.E., Didrickson, S., Kobayashi, T., Knight, M., Johnson, R.S., (2001). Hypoxia in cartilage:

HIF-1alpha is essential for chondrocyte growth arrest and survival. *Genes Dev.*, **15** (21), 2865–2876.

[25] Maes, C., Kobayashi, T., Selig, M.K., Torrekens, S., Roth, S.I., Mackem, S., Carmeliet, G., Kronenberg, H.M., (2010). Osteoblast precursors, but not mature osteoblasts, move into developing and fractured bones along with invading blood vessels. *Dev. Cell*, **19**, 329–344.

[26] Vu, T.H., Shipley, J.M., Bergers, G., Berger, J.E., Helms, J.A., Hanahan, D., Shapiro, S.D., Senior, R.M., Werb, Z., (1998). MMP-9/gelatinase B is a key regulator of growth plate angiogenesis and apoptosis of hypertrophic chondrocytes. *Cell*, **93** (3), 411–422.

[27] Stickens, D., Behonick, D.J., Ortega, N., Heyer, B., Hartenstein, B., Yu, Y., Fosang, A.J., Schorpp-Kistner, M., Angel, P., Werb, Z., (2004). Altered endochondral bone development in matrix metalloproteinase 13-deficient mice. *Development*, **131** (23), 5883–5895.

[28] Bord, S., Horner, A., Beeton, C.A., Hembry, R.M., Compston, J.E., (1999). Tissue inhibitor of matrix metalloproteinase-1 (TIMP-1) distribution in normal and pathological human bone. *Bone*, **24** (3), 229–235.

[29] Apte, S.S., Fukai, N., Beier, D.R., Olsen, B.R., (1997). The matrix metalloproteinase-14 (MMP-14) gene is structurally distinct from other MMP genes and is co-expressed with the TIMP-2 gene during mouse embryogenesis. *J. Biol. Chem.*, **272** (41), 25511–25517.

[30] Apte, S.S., Hayashi, K., Seldin, M.F., Mattei, M.-G., Hayashi, M., Olsen, B.R., (1994). Gene encoding a novel murine tissue inhibitor of metalloproteinases (TIMP), TIMP-3, is expressed in developing mouse epithelia, cartilage, and muscle, and is located on mouse chromosome 10. *Dev. Dyn.*, **200** (3), 177–197.

[31] Poulet, B., Liu, K.e., Plumb, D., Vo, P., Shah, M., Staines, K., Sampson, A., Nakamura, H., Nagase, H., Carriero, A., Shefelbine, S., Pitsillides, A.A., Bou-Gharios, G., Zhang, C., (2016). Overexpression of TIMP-3 in chondrocytes produces transient reduction in growth plate length but permanently reduces adult bone quality and quantity. *PLoS ONE*, **11** (12), e0167971.

[32] Masuyama, R., Stockmans, I., Torrekens, S., Van Looveren, R., Maes, C., Carmeliet, P., Bouillon, R., Carmeliet, G., (2006). Vitamin D receptor in chondrocytes promotes osteoclastogenesis and regulates FGF23 production in osteoblasts. *J Clin Invest*, **116** (12), 3150–3159.

[33] Xiong, J., Onal, M., Jilka, R.L., Weinstein, R.S., Manolagas, S.C., O'Brien, C.A., (2011). Matrix-embedded cells control osteoclast formation. *Nat. Med.*, **17** (10), 1235–1241.

[34] Tsang, K.Y., Chan, D., Cheah, K.S., (2015). Fate of growth plate hypertrophic chondrocytes: death or lineage extension? *Dev. Growth Differ.*, **57**, 179–192.

[35] Amizuka, N., Hasegawa, T., Oda, K., Luiz de Freitas, P.H., Hoshi, K., Li, M., Ozawa, H., (2012). Histology of epiphyseal cartilage calcification and endochondral ossification. *Front. Biosci. (Elite Ed)*, **4**, 2085–2100.

[36] Colnot, C., de la Fuente, L., Huang, S., Hu, D., Lu, C., St-Jacques, B., Helms, J.A., (2005). Indian hedgehog synchronizes skeletal angiogenesis and perichondrial maturation with cartilage development. *Development*, **132** (5), 1057–1067.

[37] Komori, T., Yagi, H., Nomura, S., Yamaguchi, A., Sasaki, K., Deguchi, K., Shimizu, Y., Bronson, R.T., Gao, Y.-H., Inada, M., Sato, M., Okamoto, R., Kitamura, Y., Yoshiki, S., Kishimoto, T., (1997). Targeted disruption of Cbfa1 results in a complete lack of bone formation owing to maturational arrest of osteoblasts. *Cell*, **89** (5), 755–764.

[38] Otto, F., Thornell, A.P., Crompton, T., Denzel, A., Gilmour, K.C., Rosewell, I.R., Stamp, G.W., Beddington, R.S., Mundlos, S., Olsen, B.R., Selby, P.B., Owen, M.J., (1997). Cbfa1, a candidate gene for cleidocranial dysplasia syndrome, is essential for osteoblast differentiation and bone development. *Cell*, **89**, 765–771.

[39] Choi, J.Y., Pratap, J., Javed, A., Zaidi, S.K., Xing, L., Balint, E., Dalamangas, S., Boyce, B., van Wijnen, A.J., Lian, J.B., Stein, J.L., Jones, S.N., Stein, G.S., (2001). Subnuclear targeting of RunxyCbfayAML factors is essential for tissue-specific differentiation during embryonic development. *PNAS*, **98**, 8650–8655.

[40] Ueta, C., Iwamoto, M., Kanatani, N., Yoshida, C., Liu, Y., Enomoto-Iwamoto, M., Ohmori, T., Enomoto, H., Nakata, K., Takada, K., Kurisu, K., Komori, T., (2001). Skeletal malformations caused by overexpression of Cbfa1 or its dominant negative form in chondrocytes. *J. Cell Biol.*, **153** (1), 87–100.

[41] Takeda, S., Bonnamy, J.P., Owen, M.J., Ducy, P., Karsenty, G., (2001). Continuous expression of Cbfa1 in nonhypertrophic chondrocytes uncovers its ability to induce hypertrophic chondrocyte differentiation and partially rescues Cbfa1-deficient mice. *Genes Dev.*, **15** (4), 467–481.

[42] Catheline, S.E., Hoak, D., Chang, M., Ketz, J.P., Hilton, M. J., Zuscik, M.J., Jonason, J.H., (2019). Chondrocyte-Specific RUNX2 overexpression accelerates post-traumatic osteoarthritis progression in adult mice. *J. Bone Miner. Res.*, **34** (9), 1676–1689.

[43] Ding, M., Lu, Y., Abbassi, S., Li, F., Li, X., Song, Y., Geoffroy, V., Im, H.-J., Zheng, Q., (2012). Targeting Runx2 expression in hypertrophic chondrocytes impairs endochondral ossification during early skeletal development. *J. Cell. Physiol.*, **227** (10), 3446–3456.

[44] Takarada, T., Hinoi, E., Nakazato, R., Ochi, H., Xu, C., Tsuchikane, A., Takeda, S., Karsenty, G., Abe, T., Kiyonari, H., Yoneda, Y., (2013). An analysis of skeletal development in osteoblast-specific and chondrocyte-specific runt-related transcription factor-2 (Runx2) knockout mice. *J. Bone Miner. Res.*, **28** (10), 2064–2069.

[45] Gebhard, S., Hattori, T., Bauer, E., Schlund, B., Bösl, M. R., de Crombrugghe, B., von der Mark, K., (2008). Specific expression of Cre recombinase in hypertrophic cartilage under the control of a BAC-Col10a1 promoter. *Matrix Biol.*, **27** (8), 693–699.

[46] H.M. Kronenberg, PTHrP and skeletal development, Ann. N.Y. Acad. Sci., 1068 (2006) 1-13.

[47] Karaplis, A.C., Luz, A., Glowacki, J., Bronson, R.T., Tybulewicz, V.L., Kronenberg, H.M., Mulligan, R.C., (1994). Lethal skeletal dysplasia from targeted disruption of the parathyroid hormone-related peptide gene. *Genes Dev.*, **8** (3), 277–289.

[48] Inada, M., Yasui, T., Nomura, S., Miyake, S., Deguchi, K., Himeno, M., Sato, M., Yamagiwa, H., Kimura, T., Yasui, N., Ochi, T., Endo, N., Kitamura, Y., Kishimoto, T., Komori, T., (1999). Maturational disturbance of chondrocytes in Cbfa1-deficient mice. *Dev. Dyn.*, **214** (4), 279–290.

[49] Pratap, J., Wixted, J.J., Gaur, T., Zaidi, S.K., Dobson, J., Gokul, K.D., Hussain, S., van Wijnen, A.J., Stein, J.L., Stein, G.S., Lian, J.B., (2008). Runx2 transcriptional activation of Indian Hedgehog and a downstream bone

metastatic pathway in breast cancer cells. *Cancer Res.*, **68** (19), 7795–7802.

[50] Qin, X., Jiang, Q., Nagano, K., Moriishi, T., Miyazaki, T., Komori, H., Ito, K., Mark, K.V.D., Sakane, C., Kaneko, H., Komori, T., (2020). Runx2 is essential for the transdifferentiation of chondrocytes into osteoblasts. *PLoS Genet.*, **16** (11), e1009169.

[51] Dao, D.Y., Jonason, J.H., Zhang, Y., Hsu, W., Chen, D.i., Hilton, M.J., O'Keefe, R.J., (2012). Cartilage-specific β-catenin signaling regulates chondrocyte maturation, generation of ossification centers, and perichondrial bone formation during skeletal development. *J. Bone Miner. Res.*, **27** (8), 1680–1694.

[52] Amling, M., Neff, L., Tanaka, S., Inoue, D., Kuida, K., Weir, E., Philbrick, W.M., Broadus, A.E., Baron, R., (1997). Bcl-2 lies downstream of parathyroid hormone-related peptide in a signaling pathway that regulates chondrocyte maturation during skeletal development. *J. Cell Biol.*, **136** (1), 205–213.

[53] Zaman, F., Chrysis, D., Huntjens, K., Fadeel, B., Sävendahl, L., Bobé, P., (2012). Ablation of the pro-apoptotic protein Bax protects mice from glucocorticoid-induced bone growth impairment. *PLoS ONE*, **7** (3), e33168.

[54] Eliseev, R.A., Dong, Y.-F., Sampson, E., Zuscik, M.J., Schwarz, E.M., O'Keefe, R.J., Rosier, R.N., Drissi, M.H., (2008). Runx2-mediated activation of the Bax gene increases osteosarcoma cell sensitivity to apoptosis. *Oncogene*, **27** (25), 3605–3614.

[55] Browne, G., Nesbitt, H., Ming, L., Stein, G.S., Lian, J.B., McKeown, S.R., Worthington, J., (2012). Bicalutamide-induced hypoxia potentiates RUNX2-mediated Bcl-2 expression resulting in apoptosis resistance. *Br. J. Cancer*, **107** (10), 1714–1721.

[56] Watanabe, H., Kimata, K., Line, S., Strong, D., Gao, L.Y., Kozak, C.A., Yamada, Y., (1994). Mouse cartilage matrix deficiency (cmd) caused by a 7 bp deletion in the aggrecan gene. *Nat. Genet.*, **7** (2), 154–157.

[57] Li, S.W., Prockop, D.J., Helminen, H., Fässler, R., Lapveteläinen, T., Kiraly, K., Peltarri, A., Arokoski, J., Lui, H., Arita, M., et al., (1995). Transgenic mice with targeted inactivation of the Col2 alpha 1 gene for collagen II develop a skeleton with membranous and periosteal bone but no endochondral bone. *Genes Dev.*, **9** (22), 2821–2830.

[58] Ortega, N., Behonick, D.J., Werb, Z., (2004). Matrix remodeling during endochondral ossification. *Trends Cell Biol.*, **14** (2), 86–93.

[59] Lausch, E., Keppler, R., Hilbert, K., Cormier-Daire, V., Nikkel, S., Nishimura, G., Unger, S., Spranger, J., Superti-Furga, A., Zabel, B., (2009). Mutations in MMP9 and MMP13 determine the mode of inheritance and the clinical spectrum of metaphyseal anadysplasia. *Am. J. Hum. Genet.*, **85** (2), 168–178.

[60] Kennedy, A.M., Inada, M., Krane, S.M., Christie, P.T., Harding, B., López-Otín, C., Sánchez, L.M., Pannett, A.A., Dearlove, A., Hartley, C., Byrne, M.H., Reed, A.A., Nesbit, M.A., Whyte, M.P., Thakker, R.V., (2005). MMP13 mutation causes spondyloepimetaphyseal dysplasia, Missouri type (SEMD(MO). *J Clin Invest*, **115** (10), 2832–2842.

[61] Verma, P., Dalal, K., (2011). ADAMTS-4 and ADAMTS-5: key enzymes in osteoarthritis. *J. Cell. Biochem.*, **12** (12), 3507–3514.

[62] Stanton, H., Rogerson, F.M., East, C.J., Golub, S.B., Lawlor, K.E., Meeker, C.T., Little, C.B., Last, K., Farmer, P.J., Campbell, I.K., Fourie, A.M., Fosang, A.J., (2005). ADAMTS5 is the major aggrecanase in mouse cartilage in vivo and in vitro. *Nature*, **434** (7033), 648–652.

[63] Glasson, S.S., Askew, R., Sheppard, B., Carito, B., Blanchet, T., Ma, H.L., Flannery, C.R., Peluso, D., Kanki, K., Yang, Z., Majumdar, M.K., Morris, E.A., (2005). Deletion of active ADAMTS5 prevents cartilage degradation in a murine model of osteoarthritis. *Nature*, **434** (7033), 644–648.

[64] Rogers-DeCotes, A.W., Porto, S.C., Dupuis, L.E., Kern, C. B., (2021). ADAMTS5 is required for normal trabeculated bone development in the mandibular condyle. *Osteoarthritis Cartilage*, **2** (4), 547–557.

[65] Rajasekaran, S., Kanna, R.M., Senthil, N., Raveendran, M., Ranjani, V., Cheung, K.M., Chan, D., Kao, P.K., Yee, A., Shetty, A.P., (2015). Genetic susceptibility of lumbar degenerative disc disease in young Indian adults. *Eur. Spine J.*, **24** (9), 1969–1975.

[66] Hirata, M., Kugimiya, F., Fukai, A., Saito, T., Yano, F., Ikeda, T., Mabuchi, A., Sapkota, B.R., Akune, T., Nishida, N., Yoshimura, N., Nakagawa, T., Tokunaga, K., Nakamura, K., Chung, U.I., Kawaguchi, H., (2012). C/EBPbeta and RUNX2 cooperate to degrade cartilage with MMP-13 as the target and HIF- 2alpha as the inducer in chondrocytes. *Hum. Mol. Genet.*, **21** (5), 1111–1123.

[67] Pratap, J., Javed, A., Languino, L.R., van Wijnen, A.J., Stein, J.L., Stein, G.S., Lian, J.B., (2005). The Runx2 osteogenic transcription factor regulates matrix metalloproteinase 9 in bone metastatic cancer cells and controls cell invasion. *Mol. Cell. Biol.*, **25** (19), 8581–8591.

[68] Thirunavukkarasu, K., Pei, Y., Moore, T.L., Wang, H., Yu, X.P., Geiser, A.G., Chandrasekhar, S., (2006). Regulation of the human ADAMTS-4 promoter by transcription factors and cytokines. *Biochem. Biophys. Res. Commun.*, **345** (1), 197–204.

[69] Thirunavukkarasu, K., Pei, Y., Wei, T., (2007). Characterization of the human ADAMTS-5 (aggrecanase-2) gene promoter. *Mol. Biol. Rep.*, **34** (4), 225–231.

[70] Jackson, H.W., Defamie, V., Waterhouse, P., Khokha, R., (2017 Jan). TIMPs: versatile extracellular regulators in cancer. *Nat. Rev. Cancer*, **17** (1), 38–53. https://doi.org/10.1038/nrc.2016.115. Epub 2016 Dec 9 PMID: 27932800.

[71] Cawston, T.E., Murphy, G., Mercer, E., Galloway, W.A., Hazleman, B.L., Reynolds, J.J., (1983). The interaction of purified rabbit bone collagenase with purified rabbit bone metalloproteinase inhibitor. *Biochem. J.*, **211** (2), 313–318.

[72] Saw, S., Aiken, A., Fang, H., McKee, T.D., Bregant, S., Sanchez, O., Chen, Y., Weiss, A., Dickson, B.C., Czarny, B., Sinha, A., Fosang, A., Dive, V., Waterhouse, P.D., Kislinger, T., Khokha, R., (2019). Metalloprotease inhibitor TIMP proteins control FGF-2 bioavailability and regulate skeletal growth. *J. Cell Biol.*, **218** (9), 3134–3152.

[73] Clark, I.M., Swingler, T.E., Sampieri, C.L., Edwards, D.R., (2008). The regulation of matrix metalloproteinases and their inhibitors. *Int. J. Biochem. Cell Biol.*, **40** (6–7), 1362–1378.

[74] Bertrand-Philippe, M., Ruddell, R.G., Arthur, M.J., Thomas, J., Mungalsingh, N., Mann, D.A., (2008). Regulation of tissue inhibitor of metalloproteinase 1 gene transcription by Runx1 and Runx2. *J. Biol. Chem.*, **279** (23), 24530–24539.

[75] Kishimoto, K., Kitazawa, R., Kurosaka, M., Maeda, S., Kitazawa, S., (2006). Expression profile of genes related to osteoclastogenesis in mouse growth plate and articular cartilage. *Histochem. Cell Biol.*, **125** (5), 593–602.

[76] Kearns, A.E., Khosla, S., Kostenuik, P.J., (2008). Receptor activator of nuclear factor kappaB ligand and osteoprotegerin regulation of bone remodeling in health and disease. *Endocr. Rev.*, **29** (2), 155–192.

[77] Enomoto, H., Shiojiri, S., Hoshi, K., Furuichi, T., Fukuyama, R., Yoshida, C.A., Kanatani, N., Nakamura, R., Mizuno, A., Zanma, A., Yano, K., Yasuda, H., Higashio, K., Takada, K., Komori, T., (2003). Induction of osteoclast differentiation by Runx2 through receptor activator of nuclear factor-kappa B ligand (RANKL) and osteoprotegerin regulation and partial rescue of osteoclastogenesis in $Runx2^{-/-}$ mice by RANKL transgene. *J. Biol. Chem.*, **278** (26), 23971–23977.

[78] Madisen, L., Zwingman, T.A., Sunkin, S.M., Oh, S.W., Zariwala, H.A., Gu, H., Ng, L.L., Palmiter, R.D., Hawrylycz, M.J., Jones, A.J., Lein, E.S., Zeng, H., (2010). A robust and high-throughput Cre reporting and characterization system for the whole mouse brain. *Nat. Neurosci.*, **13** (1), 133–140.

[79] Adhami, M.D., Rashid, H., Chen, H., Clarke, J.C., Yang, Y., Javed, A., (2015). Loss of Runx2 in committed osteoblasts impairs postnatal skeletogenesis. *J. Bone Miner. Res.*, **30** (1), 71–82.

[80] H. Rashid, H. Chen, Q. Hassan, A. Javed, Dwarfism in homozygous $Agc1^{CreERT}$ mice is associated with decreased expression of aggrecan, Genesis 55(10) (2017) 10.1002.